2012-9-27

High-Spin Structure of ^{95}Pd

Raluca Mărginean, *et al.*

High-spin structure of ^{95}Pd

R. Mărginean,[1] C. Rusu,[2] N. Mărginean,[1] D. Bucurescu,[1] C. A. Ur,[1,3] G. de Angelis,[4] M. Axiotis,[5] D. Bazzacco,[3] E. Farnea,[3] A. Gadea,[6] M. Ionescu-Bujor,[1] A. Iordăchescu,[1] W. Krolas,[7] Th. Kröll,[8] S. M. Lenzi,[3] S. Lunardi,[3] D. R. Napoli,[4] C. Rossi Alvarez,[3] and J. Wrzesinski[7]

[1]*Horia Hulubei National Institute for Physics and Nuclear Engineering, Bucharest, Romania*
[2]*University of Texas at Dallas, School of Natural Sciences and Mathematics, Richardson, Texas, USA*
[3]*Dipartimento di Fisica dell' Università and INFN, Sezione di Padova, Padova, Italy*
[4]*INFN, Laboratori Nazionali di Legnaro, Legnaro, Italy*
[5]*Institute of Nuclear Physics, NCSR Demokritos, Aghia Paraskevi, Greece*
[6]*Universitat de Vàlencia, IFIC CSIC, E-46100 Burjassot, Valencia, Spain*
[7]*H. Niewodniczanski Institute of Nuclear Physics PAN, PL-31342 Krakow, Poland*
[8]*Institut für Kernphysik, Technische Universität Darmstadt, 64289 Darmstadt, Germany*

(Received 15 May 2012; revised manuscript received 7 August 2012; published 27 September 2012)

The level scheme of the neutron-deficient nucleus ^{95}Pd has been studied with the ^{58}Ni + ^{40}Ca fusion-evaporation reaction at 135 MeV with the GASP γ-ray array, the ISIS silicon ball, and the N-ring neutron detector. Excited levels with spins at least up to $\frac{45}{2}\hbar$ are reported for both parities. The observed experimental data are compared to large-scale shell-model calculations.

DOI: 10.1103/PhysRevC.86.034339 PACS number(s): 21.10.−k, 23.20.Lv, 21.60.Cs, 27.60.+j

I. INTRODUCTION

The neutron-deficient $N \lesssim 50$ nuclei near the $N = Z$ line have been the subject of intensive studies. The theoretical approaches in this nuclear region took advantage of the nearby shell closures at $N = Z = 50$ as well as the approximate closure at $Z = 38$, making shell-model calculations more feasible if only the $p_{1/2}$ and $g_{9/2}$ orbitals are considered. Earlier shell-model studies [1,2] of nuclei with $N \lesssim 50$ and $38 \leqslant Z \leqslant 50$ assumed an inert ^{88}Sr core and placed the valence protons and neutron holes in the $p_{1/2}$ and $g_{9/2}$ orbitals, but in later investigations the doubly magic nucleus ^{100}Sn was selected as core because it allows for a more symmetric treatment of protons and neutrons [3]. The good results of the previous shell-model investigations in the $(p_{1/2}, g_{9/2})$ space can be attributed to the successful determination of some effective-interaction Hamiltonians, with the matrix elements derived by least-squares fitting to experimental low- and intermediate-energy levels of nuclei with $N = 47$ to 50 [1,2,4,5]. On the other hand, as new experimental data on states with higher spins and energies become available, shell-model investigations should include extended configurations, considering single-particle excitations involving orbitals outside the restricted $(p_{1/2}, g_{9/2})$ space. In order to test and improve the effective interactions, new accurate experimental information is definitely needed, and extensive efforts must be dedicated to obtain detailed experimental data, especially for the $Z \approx N \lesssim 50$ nuclei, since these are relatively far from the line of stability and harder to study by experiments.

The ^{95}Pd nucleus is in this mass region of interest and has been previously investigated in experiments using fusion-evaporation reactions [6–10]. Many of the levels found in these experiments had no unambiguous spin and parity assignments. In our previous work [10], we reported on the low-energy part of the level scheme, experimentally confirming the theoretical predictions regarding the existence of a $21/2^+$ spin-gap isomer in ^{95}Pd, by showing that its excitation energy is just 3 keV below that of the $17/2^+$ yrast state. This was possible by linking this level to higher-lying levels whose decay could be followed down to the ground state. By finding the excitation energy of the $17/2^+$ level, the energies of the previously known levels decaying to this state were also correctly assigned. The observed structure at energies below 5 MeV was previously well described by shell-model calculations [10] performed using the model space as described in Ref. [4]. The present work presents new information on the nuclear structure of the ^{95}Pd nucleus, by extending the level scheme towards states with higher spin and excitation energy. In order to better understand the newly observed structures, new shell-model calculations were performed with an extended configuration space built on the $\pi\nu(f, p, g, d, s, h_{11/2})$ orbitals.

II. EXPERIMENT

The ^{95}Pd nucleus was populated in the $2pn$ channel of the ^{58}Ni + ^{40}Ca fusion-evaporation reaction performed at the Legnaro XTU Tandem accelerator. The incident beam energy of 135 MeV was chosen to favor the two- and three-particle evaporation channels. The beam intensity during the experiment was about 8 particle nA, and a ^{58}Ni foil of thickness 6 mg/cm^2 was used as a target. The γ rays were detected with the GASP detector array [11] arranged in its standard configuration with 40 Compton-suppressed HPGe detectors and an 80-element bismuth-germanate (BGO) inner ball. The trigger condition required at least two Ge detectors and one BGO element firing in coincidence. The six elements of the most forward ring of the BGO inner ball were replaced by the N-ring detector [12], consisting of six BC501A liquid scintillator detectors, which were used for neutron-γ discrimination by setting in the offline analysis conditions on the pulse shape, detected energy, and time of flight. The ISIS silicon ball [13], an array of 40 E-ΔE telescopes fitting within GASP, was also used in order to have

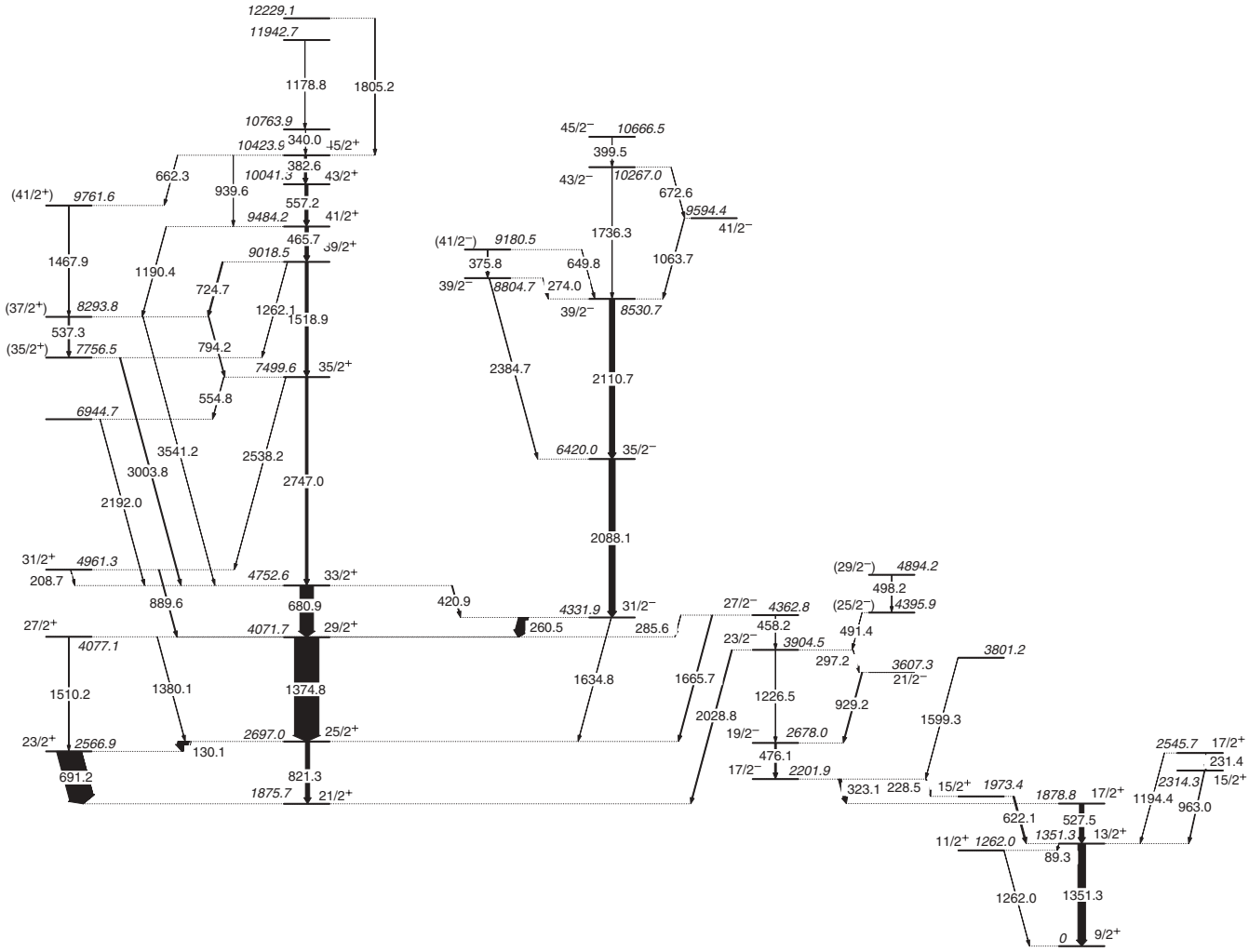

FIG. 1. Level scheme of ^{95}Pd as obtained from the present data (see Table I for details). The lower-energy part (up to the 4961.3 keV state) is identical to that presented in Ref. [10].

information (type and multiplicity) on the charged particles. The experimental values of the particle detection efficiencies were 60% for detecting one proton, 38% for one α particle, and 3.5% for one neutron. About 10^9 events were collected during the experiment. The data were sorted into γ-γ-γ coincidence cubes and γ-γ coincidence matrices under different conditions on the detected charged particles and neutrons. This allowed the assignment of the γ rays emitted in the decay of excited states to the desired residual nuclei.

III. EXPERIMENTAL RESULTS

The γ-ray transitions that belong to the decay of excited states in ^{95}Pd were assigned both by starting from previously known transitions and by examining spectra and matrices with different conditions on the detected particles. Thus, a γ ray belongs to ^{95}Pd if it is present in the γ-γ matrices built in coincidence with 0, 1, or 2 protons and neutrons, and it is not present in the matrices built upon the coincidence γ-γ with 3 or more protons or with α particles. The level scheme of ^{95}Pd, as determined in the present experiment, was mainly built by investigating the γ-γ coincidence relationships in a matrix obtained in coincidence with protons (1 or 2) and neutrons. This level scheme including also the previously reported levels [10] is shown in Fig. 1.

Spectra gated on some previously known γ rays are presented in Figs. 2 and 3, showing mainly the new γ-ray transitions depopulating the assigned negative-parity bands (Fig. 2) or the positive-parity bands (Fig. 3). Previously assigned transitions (some of them tentative) are confirmed, and, in addition, new levels are found in the higher-spin part, reaching spins of at least $\frac{45}{2}\hbar$. The excitation energies of the previously known levels were corrected, based on the accurate determination of the energy of the $21/2^+$ level as described in Ref. [10]. The position of many states in the level scheme is verified by the identification of crossing transitions between bands.

The multipolarity of the transitions were determined by analyzing both directional correlation orientation (DCO) ratios and angular distributions of the γ rays.

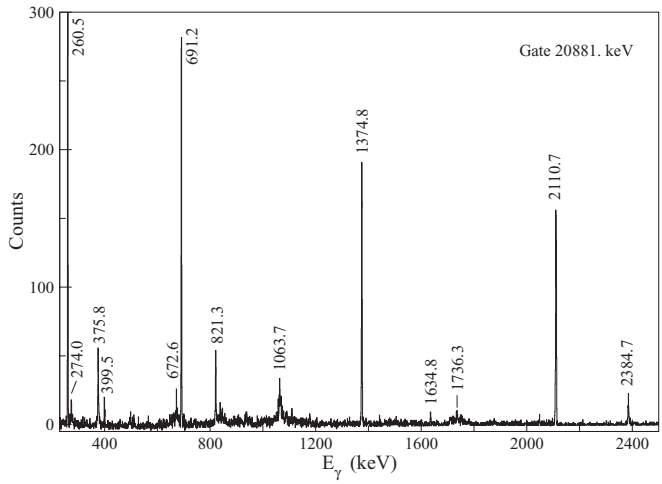

FIG. 2. Part of the spectrum gated by the 2088.1 keV transition ($35/2^- \rightarrow 31/2^-$), showing the new γ-ray transitions depopulating the high-spin negative-parity levels of ^{95}Pd.

The DCO ratios were deduced from an asymmetric γ-γ-$2p$-n matrix in which the energy of the γ rays detected in the detector rings at 35° or 145° were recorded on one axis, while that of the γ rays detected at 90° were recorded on the other axis. The definition of the DCO ratio is

$$R_{\mathrm{DCO}} = \frac{I_\gamma(35^\circ, 145^\circ)\,|_{\mathrm{gate}=90^\circ}}{I_\gamma(90^\circ)\,|_{\mathrm{gate}=35^\circ,145^\circ}},$$

where I_γ is the intensity of the transition of interest obtained by gating on a coincident transition of known multipolarity.

In the specified geometry, the value of R_{DCO} of a pure quadrupole transition should be about 1.0 when gating on a quadrupole transition and about 2.0 when gating on a stretched dipole one, while for a pure dipole transition it is about 1.0 or 0.5 when gating on a dipole or a quadrupole transition, respectively. The DCO values were determined by starting with gates on transitions of previously known multipolarity that depopulate low-energy levels. This way, spin and parity values

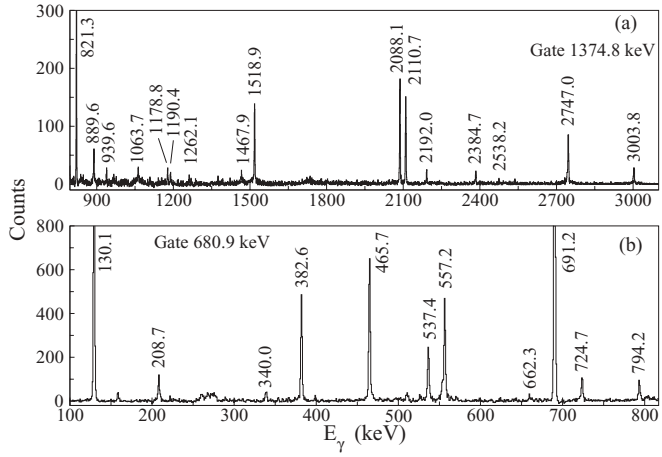

FIG. 3. Details of the spectra gated by (a) the 1374.8 keV ($29/2^+ \rightarrow 25/2^+$) transition, and (b) the 680.9 keV ($33/2^+ \rightarrow 29/2^+$) transition, showing the new transitions depopulating the positive parity levels of ^{95}Pd.

could be assigned for the majority of levels, by assuming, as usual, that the spin generally increases with increasing excitation energy.

For some of the γ transitions it was not possible to determine the DCO ratio because of the low intensity or a large Doppler shift. For these transitions, in order to estimate the multipolarity, angular distributions were extracted from the spectra of the seven rings of GASP (35°, 60°, 72°, 90°, 108°, 120°, and 145°). Since the GASP array has many detectors, placed at many different angles, the angular correlation effects between any two γ rays are washed out, so that the intensity of any γ ray in the seven rings does not depend on the character of the gating transition(s), but follows the regular angular distribution of γ rays from oriented nuclei [14].

In this respect, seven asymmetric γ-γ matrices corresponding to the coincidence of the detectors from an angular ring of GASP with the rest of all the other detectors were created. Clean γ-ray spectra were obtained from these matrices by gating on the all-detector axis, on a number of ^{95}Pd transitions, and they were corrected for the efficiency of the corresponding ring of detectors. From a Legendre polynomial analysis of the angular distributions, experimental values a_2/a_0 and a_4/a_0 were deduced.

For the level at 9761.6 keV, due to poor statistics, no spin assignment was possible by analyzing the DCO ratios or angular distribution coefficients. The spin of this level was assigned based on the "weak" argument that, since the feeding and decaying transitions connect the states above and below with a spin difference of four units, and since a combination of a dipole and an octupole transition in cascade to make up these four spin units would be very unusual, it is highly probable that the two transitions are of quadrupole type and the spin of this level is $\frac{41}{2}\hbar$.

Table I contains information on all γ rays assigned as transitions in the level scheme of ^{95}Pd, including R_{DCO} values and the corresponding gate from which it was extracted, and the obtained a_2/a_0 and a_4/a_0 values. The transition intensities normalized to the 1351.3 keV transition intensity are also presented. Figure 4 shows the DCO ratio values (deduced when gating on stretched quadrupole transitions) and the a_2/a_0 coefficients for the majority of the transitions listed in Table I. One can observe that the dipole-assigned transitions group around $R_{\mathrm{DCO}} = 0.5$ and negative a_2/a_0 values, whereas the quadrupole assigned ones have R_{DCO} around 1.0 and positive a_2/a_0 values (around 0.3–0.4).

Besides the spin-gap isomeric state $21/2^+$ at 1875.7 keV [10], the $31/2^-$ state, whose excitation energy has been assigned in the present work to be 4331.9 keV (see Fig. 1), was previously found to be isomeric, with a half-life of 12(3) ns [9]. We determined its lifetime by examining matrices of the $N(E_\gamma, t)$ type, where E_γ is the energy of one transition detected in one HPGe detector, and t is the time with respect to other γ rays detected by the BGO array [11]. By gating on the energy of a certain transition feeding or depopulating a level, one gets a time distribution that contains information on its half-life. The sequence of γ rays deexciting the $31/2^-$ isomer to lower levels contains two strong transitions at 691.2 and 1374.8 keV, with time distributions displaying long tails characteristic for a half-life in the order of 10 ns (see

TABLE I. The γ-ray transitions in ^{95}Pd, as found in the present work, associated to the level scheme shown in Fig. 1. The transition intensities are normalized to that of the 1351.3 keV γ ray, taken as 100. The excitation energy of the initial level is given in the third column, followed by the spin-parity values assigned to the initial and final levels. The next column shows the characteristics of the gating transition used for analyzing the DCO ratio. The last two columns show the angular distribution coefficients determined from the Legendre polynomial fit $W(\theta) = a_0 + a_2 P_2(\cos\theta) + a_4 P_4(\cos\theta)$.

E_γ	I_γ	Assignment			DCO gate	$R_{\rm DCO}$	a_2/a_0	a_4/a_0
(keV)		E_x(level)	$J_i^{\Pi_i}$	$J_f^{\Pi_f}$	(E_γ/mult.)			
89.3	1.2(4)	1351.3	$13/2^+$	$11/2^+$				
130.1	143.6(80)	2697.0	$25/2^+$	$23/2^+$	1374.8/Q	0.77(11)	−0.32(4)	0.04(7)
208.7	4.8(10)	4961.3	$31/2^+$	$33/2^+$	1374.8/Q	0.66(27)	−0.74(23)	−0.39(35)
228.5	10.2(21)	2201.9	$17/2^-$	$15/2^+$	1351.3/Q	0.82(24)	−0.10(12)	0.09(21)
231.4	3.3(5)	2545.7	$17/2^+$	$15/2^+$	1351.3/Q	1.1(3)		
260.5	124.1(28)	4331.9	$31/2^-$	$29/2^+$	1374.8/Q	0.55(8)	−0.30(3)	−0.17(6)
274.0	2.5(5)	8804.7	$39/2^-$	$39/2^-$	260.5/D	1.02(24)	−0.26(14)	0.16(24)
285.6	2.2(10)	4362.8	$27/2^-$	$27/2^+$				
297.2	4.4(7)	3904.5	$23/2^-$	$21/2^-$	1351.3/Q	0.35(18)	−0.32(29)	0.11(48)
323.1	38.1(36)	2201.9	$17/2^-$	$17/2^+$	1351.3/Q	1.13(23)	0.33(8)	0.00(13)
340.0	2.8(4)	10763.9		$45/2^+$				
375.8	10.8(12)	9180.5	$(41/2^-)$	$39/2^-$	1374.8/Q	0.25(17)	−0.22(16)	−0.05(25)
382.6	32.4(28)	10423.9	$45/2^+$	$43/2^+$	1374.8/Q	0.46(15)	−0.46(11)	0.04(18)
399.5	2.8(6)	10666.5	$45/2^-$	$43/2^-$	1374.8/Q	0.38(13)	−0.72(43)	−0.53(69)
420.9	11.5(23)	4752.6	$33/2^+$	$31/2^-$	1374.8/Q	0.37(10)	−0.24(14)	0.08(22)
458.2	2.1(6)	4362.8	$27/2^-$	$23/2^-$	476.1/D	2.00(74)		
465.7	42.5(24)	9484.2	$41/2^+$	$39/2^+$	1374.8/Q	0.51(11)	−0.38(9)	0.10(15)
476.1	22.4(39)	2678.0	$19/2^-$	$17/2^-$	1351.3/Q	0.33(8)	−0.48(12)	0.09(21)
491.4	2.1(5)	4395.9	$(25/2^-)$	$23/2^-$	476.1/D	0.33(8)		
498.2	2.0(4)	4894.2	$(29/2^-)$	$(25/2^-)$	476.1/D	0.34(16)		
527.5	59.3(16)	1878.8	$17/2^+$	$13/2^+$	1351.3/Q	1.05(23)	0.25(7)	−0.02(12)
537.3	19.2(15)	8293.8	$(37/2^+)$	$(35/2^+)$	1374.8/Q	0.38(12)	−0.64(13)	0.70(22)
554.8	7.2(16)	7499.6	$35/2^+$		1374.8/Q	0.59(19)	−0.79(9)	0.0(16)
557.2	39.6(43)	10041.3	$43/2^+$	$41/2^+$	1374.8/Q	0.43(7)	−0.33(11)	0.08(18)
622.1	20.3(26)	1973.4	$15/2^+$	$13/2^+$	1351.3/Q	0.46(9)	−0.22(15)	0.29(24)
649.8	3.12(90)	9180.5	$(41/2^-)$	$39/2^-$				
662.3	3.1(11)	10423.9	$45/2^+$	$(41/2^+)$				
672.6	3.9(5)	10267.0	$43/2^-$	$41/2^-$	1374.8/Q	0.54(26)		
680.9	178.0(90)	4752.6	$33/2^+$	$29/2^+$	1374.8/Q	1.11(15)	0.36(4)	−0.15(5)
691.2	318(24)	2566.9	$23/2^+$	$21/2^+$	1374.8/Q	0.50(4)	−0.41(4)	−0.01(6)
724.7	16.5(8)	9018.5	$39/2^+$	$(37/2^+)$	1374.8/Q	0.57(29)	−0.23(15)	0.02(24)
794.2	10.4(11)	8293.8	$(37/2^+)$	$35/2^+$	1374.8/Q	0.48(21)	0.42(17)	−0.07(26)
821.3	55.6(24)	2697.0	$25/2^+$	$21/2^+$	680.9/Q	0.98(23)	0.35(9)	−0.36(13)
889.6	12.3(18)	4961.3	$31/2^+$	$29/2^+$	691.2/D	0.72(32)	−0.19(18)	0.38(28)
929.2	13.2(15)	3607.3	$21/2^-$	$19/2^-$	476.1/D	1.00(33)	−0.37(21)	0.14(33)
939.6	3.3(5)	10423.9	$45/2^+$	$41/2^+$				
963.0	8.5(6)	2314.3	$15/2^+$	$13/2^+$	1351.3/Q	0.55(19)	−0.19(19)	−0.02(32)
1063.7	7.2(9)	9594.4	$41/2^-$	$39/2^-$	1374.8/Q	0.32(14)	0.06(11)	−0.09(17)
1178.8	2.9(8)	11942.7			1374.8/Q	0.52(33)		
1190.4	5.8(7)	9484.2	$41/2^+$	$(37/2^+)$	1374.8/Q	0.62(31)		
1194.4	1.4(3)	2545.7	$17/2^+$	$13/2^+$				
1226.5	4.6(20)	3904.5	$23/2^-$	$19/2^-$				
1262.0	4.3(12)	1262.0	$11/2^+$	$9/2^+$				
1262.1	3.3(2)	9018.5	$39/2^+$	$(35/2^+)$	527.5/Q	0.80(32)		
1351.3	100.0	1351.3	$13/2^+$	$9/2^+$	527.5/Q	0.97(16)	0.39(6)	0.05(8)
1374.8	322(10)	4071.7	$29/2^+$	$25/2^+$	680.9/Q	0.87(15)	−0.10(2)	0.19(3)
1380.1	6.2(10)	4077.1	$27/2^+$	$25/2^+$	691.2/D	0.92(35)	−0.41(20)	1.16(40)
1467.9	5.1(9)	9761.6	$(41/2^+)$	$(37/2^+)$				
1510.2	4.4(7)	4077.1	$27/2^+$	$23/2^+$				
1518.9	38.4(21)	9018.5	$39/2^+$	$35/2^+$	680.9/Q	0.65(15)	0.29(10)	0.09(15)
1599.3	3.5(22)	3801.2		$17/2^-$				
1634.8	5.1(13)	4331.9	$31/2^-$	$25/2^+$				

TABLE I. (*Continued*.)

E_γ (keV)	I_γ	Assignment			DCO gate (E_γ/mult.)	R_{DCO}	a_2/a_0	a_4/a_0
		E_x(level)	$J_i^{\Pi_i}$	$J_f^{\Pi_f}$				
1665.7	12.4(31)	4362.8	$27/2^-$	$25/2^+$	691.2/D	0.94(41)	−0.14(19)	−0.11(31)
1736.3	5.6(13)	10267.0	$43/2^-$	$39/2^-$			0.24(18)	−0.38(25)
1805.2	6.4(14)	12229.1		$45/2^+$				
2028.8	13.2(38)	3904.5	$23/2^-$	$21/2^+$				
2088.1	80.9(24)	6420.0	$35/2^-$	$31/2^-$	1374.8/Q	0.64(25)	0.43(9)	0.29(13)
2110.7	68.2(23)	8530.7	$39/2^-$	$35/2^-$	1374.8/Q	1.61(39)	0.56(10)	0.25(14)
2192.0	5.7(11)	6944.7		$33/2^+$	1374.8/Q	1.67(75)	0.41(19)	0.95(30)
2384.7	7.5(9)	8804.7	$39/2^-$	$35/2^-$			0.76(31)	0.43(41)
2538.2	1.8(4)	7499.6	$35/2^+$	$31/2^+$				
2747.0	33.9(58)	7499.6	$35/2^+$	$33/2^+$	1374.8/Q	0.23(8)	−0.76(7)	0.79(15)
3003.8	12.9(18)	7756.5	$(35/2^+)$	$33/2^+$	1374.8/Q	1.34(46)	−0.10(11)	0.87(19)
3541.2	1.3(4)	8293.8	$(37/2^+)$	$33/2^+$				

Fig. 5). The time spectra shown in Fig. 5 have, besides the delayed components from coincidences with γ rays in the deexcitation sequences feeding into the $31/2^-$ isomer, prompt components coming mainly from prompt coincidences with other γ rays from decay paths bypassing the $31/2^-$ isomer. In order to extract a precise half-life value, the time spectra were fitted with a combination of Gaussian curves, representing the prompt part (identical in shape to the time-response function), a constant accounting for random coincidences, plus a delayed component given by the convolution of an exponential-decay function and the time response (for additional details on this kind of procedure, see Ref. [15]). The time-response functions characterizing prompt transitions depend on the energy. The right part of Fig. 5 shows typical time spectra with only prompt decays coincident to neutrons. They have been obtained using transitions at 696.1 and 1333.4 keV in ^{94}Rh, the 3pn channel, hence energies very similar to the transition energies of interest in ^{95}Pd. The half-life values determined for the $31/2^-$ isomer from the time spectra of the 691.2 and 1374.8 keV transitions are 11.3(10) and 11.0(10) ns, respectively, with a mean value and combined uncertainty of 11.2(7) ns, which confirms the result in Ref. [9] and is more precise.

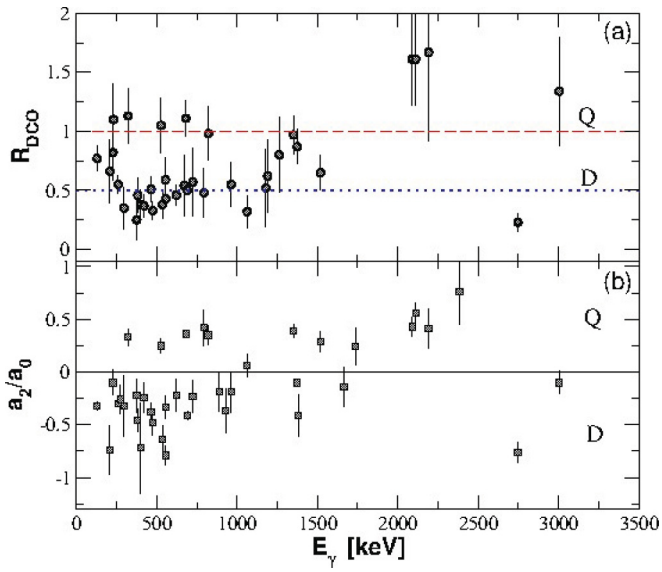

FIG. 4. (Color online) DCO ratio (a) and a_2/a_0 (b) values for ^{95}Pd transitions listed in Table I. The displayed DCO ratios are obtained when gating on quadrupole transitions.

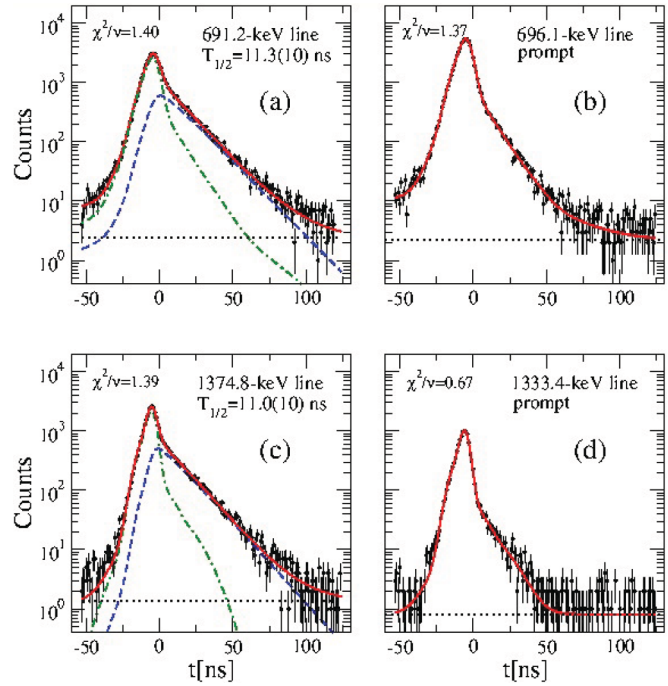

FIG. 5. (Color online) Left panels (a) and (c): Time spectra gated on the 691.2 and 1374.8 keV transitions. The filled circles are the experimental data, the continuous curves are the total fits, the dashed lines are the delayed decay curves corresponding only to the half-life of the isomeric level, and the dot-dashed curves are the prompt components of the time spectra. Right panels (b) and (d): Prompt-response curves (continuous lines) corresponding to each of the decay curves on the left side, extracted from the time spectra (filled circles) of the nearby prompt lines of ^{94}Rh (696.1 and 1333.4 keV). For all spectra, the dotted lines are the estimated background levels of accidental coincidences.

IV. COMPARISON WITH SHELL-MODEL CALCULATIONS

Shell-model calculations were previously performed within the $\pi\nu(p_{1/2}, g_{9/2})$ and $\pi(f_{5/2}, p, g_{9/2}) \otimes \nu(g_{9/2}, d_{5/2})$ model spaces using various interactions [3,5,10,16]. In this work, the shell-model calculations were carried out using the OXBASH code [17], with a configuration space larger than those used in previous shell-model studies. In order to calculate states with higher spins and to investigate the decay of the $31/2^-$ isomer, the model space was extended to include particle-hole excitations within the orbitals $\pi\nu(f, p, g, d, s, h_{11/2})$, and two empirical Hamiltonians were combined to describe the interaction between all these orbitals. The effective-interaction set F-FIT [5] was used for the interactions within the $\pi\nu(p_{1/2}, g_{9/2})$ orbitals, as this describes well many nuclei with $Z \gtrsim 40$ and $N \leqslant 50$, providing good results for most yrast and near-yrast states with enough number of particles and/or holes in the $g_{9/2}$ orbitals to generate relatively high angular momenta at low and intermediate excitation energies. All other interaction matrix elements were calculated for an oscillator length of 2.21 fm using the empirical parametrization of interaction potentials from Ref. [18] (see Table XVII in this reference). The two-body Coulomb repulsion was also included in the proton-proton part of the combined residual interaction. The extension of the model space by including all the orbitals $\pi\nu(f, p, g, d, s, h_{11/2})$ allows spurious center-of-mass (CM) excitations. To minimize the contaminations from the spurious CM motion, the CM Hamiltonian, multiplied by relatively large factors [$\alpha \times H_{CM}(\hbar\omega/A = 1$ MeV) with $\alpha = 1$, 5, 10, and 15], was added to the combined effective-interaction Hamiltonian [19]. With this kind of CM correction, the CM contaminations are not significant (<1%) for all quantities of interest reported in this work.

The single-particle energies of the orbitals used in the present calculations are shown in Fig. 6, relative to the ^{100}Sn core. The energies of the orbitals $\pi(f_{5/2}, p, g_{9/2})$ and $\nu(f_{5/2}, p, g, d, s, h_{11/2})$ were empirically adjusted so that the spin-orbit splitting of the neutron $\nu(g_{9/2}, g_{7/2})$ orbitals

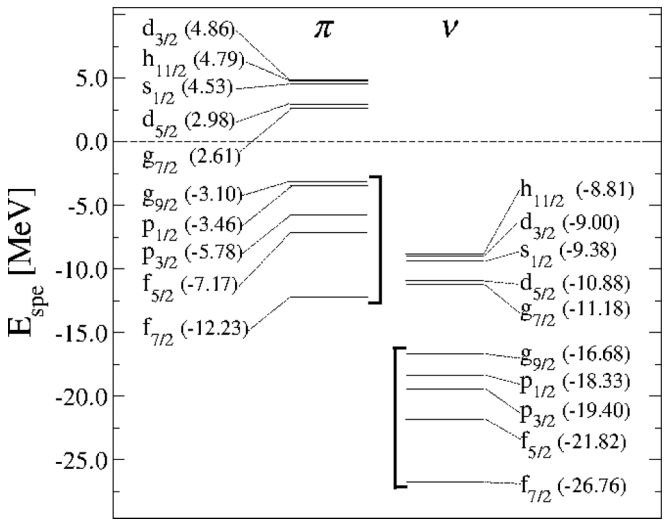

FIG. 6. Single-particle energies relative to the closed core ^{100}Sn.

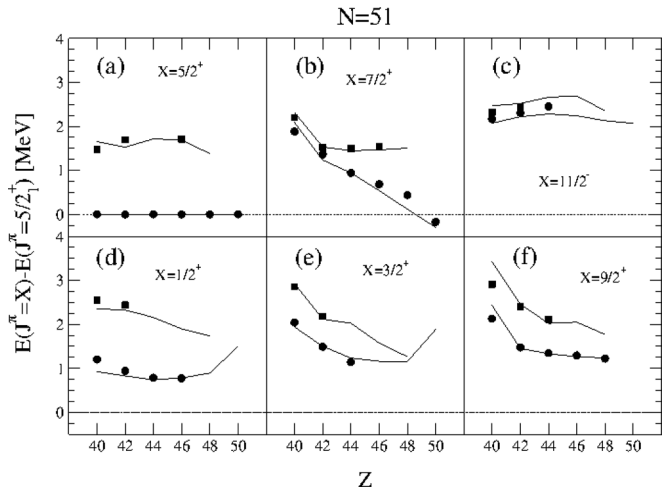

FIG. 7. Excitation energies, relative to the first $5/2^+$ state, for low-lying first (filled circles) and second (filled squares) states with the specified spin of $N = 51$ isotones in comparison with shell-model calculations (lines).

reproduces the difference in the binding energies of ^{90,91}Zr nuclei, and the low-lying levels dominated by single-particle excitations in neighboring odd-A nuclei with $N = 49$, 50, and 51 are adequately described. For example, the sequence of graphs in Fig. 7 shows that the calculated low-lying levels of nuclei with $N = 51$ are in reasonably good agreement with the experimental data. It is also worth noting in Fig. 7(b) that, due to the tensor part of the nucleon-nucleon interaction [20], the gradual filling of the $\pi g_{9/2}$ orbital leads to an increasingly strong monopole shift of the $\nu g_{7/2}$ orbital, lowering the $\nu g_{7/2}$ single-particle energy closer to that of the $\nu d_{5/2}$ orbital. As a consequence, excitations involving the $\nu d_{5/2}$ and $\nu g_{7/2}$ orbitals are expected to play an important role in the structure of nuclei in the upper half of the $Z = 40$–50 subshell. Our calculations also show that, in ^{101}Sn, the single-particle energy of the $\nu g_{7/2}$ orbital drops even lower than that of the $\nu d_{5/2}$ orbital. This inversion of the $\nu g_{7/2}$ and $\nu d_{5/2}$ orbitals in ^{101}Sn seems strongly supported by a more recent investigation of this nucleus [21], where the ground state was found as $7/2^+$ with a first excited state $5/2^+$ at 172 keV.

Unfortunately, the experimental data available for nuclei with $N \gtrsim Z$ and $A \sim 90$–95 do not bear significant information on the $\pi\nu f_{7/2}$ orbitals, and the energies of these orbitals were estimated from various Wood-Saxon, folded Yukawa potentials, and Skyrme III Hartee-Fock calculations (see, for example, Refs. [22,23]) to be about 5 MeV below the higher spin-orbit partner orbitals $\pi\nu f_{5/2}$. The energies of the proton $\pi(g_{7/2}, d, s, h_{11/2})$ orbitals were taken to be the same as those empirically deduced for neutrons, relative to the $\pi\nu g_{9/2}$ orbitals, in the absence of residual interactions. Overall, the interaction was found slightly too strong for ^{95}Pd, and a further 12% reduction was also applied.

In general, for calculating electromagnetic transitions, renormalizations of the corresponding operators should be performed to compensate for configurations missing from a truncated model space, core polarization involving virtual excitations of collective vibrations, or possible contributions

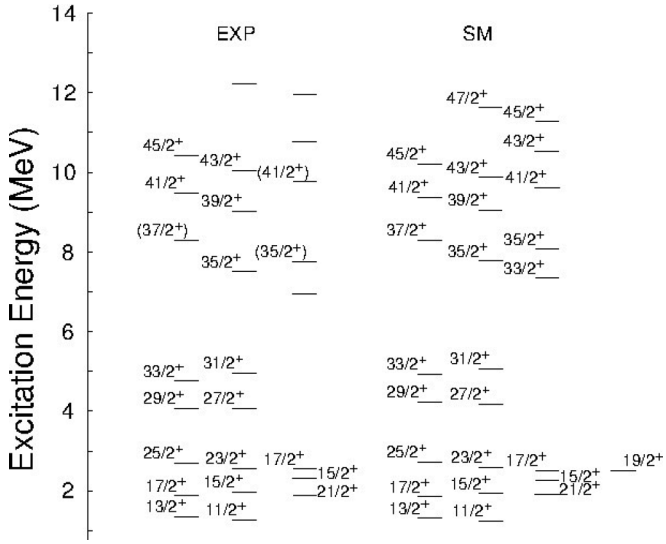

FIG. 8. Shell-model predictions for positive-parity states of ^{95}Pd in comparison with experimental levels.

from non-nucleonic degrees of freedom. In the present work, this was taken into account by using the following effective charges and g factors: $e_{\pi,\mathrm{eff}}(E1) = +0.5N/Ae$, $e_{\nu,\mathrm{eff}}(E1) = -0.5Z/Ae$, $e_{\pi,\mathrm{eff}}(E2) = +1.5e$, $e_{\nu,\mathrm{eff}}(E2) = +0.5e$, $g_{s,\mathrm{eff}} = 0.7g_{s,\mathrm{free}}$, and $g_{l,\mathrm{eff}} = g_{l,\mathrm{free}}$.

The calculated excitation energies are in reasonably good agreement with the experimental ones, as can be observed in Figs. 8 and 9. The largest discrepancy is noticed for the $35/2_1^-$ level, which is predicted at an excitation energy about 1 MeV higher than the experimental one. A similarly overestimated value has also been reported in an earlier study of ^{95}Pd [7]. The structure of the $35/2_1^-$ level is predicted as basically being an $f_{5/2}$ proton-hole state intruding into the energy gap formed between the lower-energy excitations within the $\pi\nu(p_{1/2}, g_{9/2})$ orbitals and the higher-energy neutron-hole excitations across the $N = 50$ shell closure. The $\pi f_{5/2}$ single-particle energy was

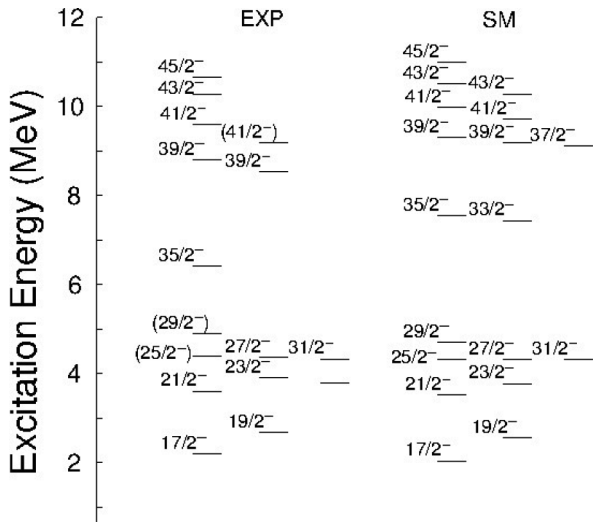

FIG. 9. Shell-model predictions for negative-parity states of ^{95}Pd in comparison with experimental levels.

determined from the known low-lying states in the $N = 50$ nuclei ^{89}Y and ^{91}Nb, which are a few mass units away from ^{95}Pd, and the relatively large discrepancy of this $35/2_1^-$ level might reflect some deficiency in the interaction involving the $\pi f_{5/2}$ orbital. In particular, the $\langle f_{5/2}, g_{9/2}|V_{\pi\nu}|f_{5/2}, g_{9/2}\rangle$ matrix elements at $T = 1$ are systematically more "repulsive" (or less "attractive") than the corresponding components of other different effective interactions [24,25]. Tuning key interaction matrix elements involving the $\pi f_{5/2}$ orbital, or simply readjusting the $\pi f_{5/2}$ single-particle energy, can improve the calculated energy of the $35/2_1^-$ level without significantly changing the calculated wave functions and energies of all other levels studied in this work

The ground state is predicted to have spin and parity $9/2^+$ and is mainly built on one neutron hole in the $\nu g_{9/2}$ orbital. The excited levels with energies below 5 MeV cluster in several groups of levels that are overwhelmingly dominated by the members of two basic configurations,[1] $\pi(g_{9/2}^{-4}) \otimes \nu(g_{9/2}^{-1})$ and $\pi(p_{1/2}^{-1}, g_{9/2}^{-3}) \otimes \nu(g_{9/2}^{-1})$, with positive and negative parity, respectively. The proton-neutron interaction, especially the strongly attractive matrix element $\langle g_{9/2}^2|V_{\pi\nu}|g_{9/2}^2\rangle_{J=9}$, favors the alignment of these configurations at $J^\pi = 21/2^+$and $31/2^-$, lowering their excitation energies and leading to the possibility of forming isomeric states below those to which they could decay by fast $M1/E2$ transitions. Even though the excitation energy of the $21/2^+$ isomer is predicted 63 keV above the first $17/2^+$ level, while, experimentally, the ordering of these two states is inverted ($E_{21/2^+} - E_{17/2^+} \simeq -3$ keV), this is hardly surprising when considering that the uncertainties in the interaction matrix elements of the F-FIT set are of the order of 100 keV. On the other hand, the $31/2_1^-$ level is correctly predicted below the $27/2_1^-$ and $29/2_1^-$ levels, as observed experimentally.

For ^{95}Pd, the maximum spins allowed, taking into account only the $\pi\nu(p_{1/2}, g_{9/2})$ orbitals, are $33/2$ and $31/2$ for positive- and negative-parity states, respectively. To construct states with higher spins, starting from the two basic configurations for the low-lying positive- and negative-parity states, $\pi(g_{9/2}^{-4}) \otimes \nu(g_{9/2}^{-1})$ and $\pi(p_{1/2}^{-1}, g_{9/2}^{-3}) \otimes \nu(g_{9/2}^{-1})$, one nucleon was allowed to "jump" from the partially or totally occupied orbitals into any higher unoccupied or partially occupied orbital. Within this extended configuration space, the positive-parity levels $33/2_2^+$, $35/2_{1,2}^+$, $37/2_1^+$, $39/2_1^+$, $41/2_{1,2}^+$, and $45/2_1^+$, with excitation energies in the 7–10 MeV range, have contributions of the dominant configuration $\pi(g_{9/2}^{-4}) \otimes \nu(g_{9/2}^{-2}, d_{5/2}^1)$ greater than 75%. The higher-energy positive-parity levels $45/2_2^+$ and $47/2_1^+$ are predicted to be almost pure members of the $\pi(g_{9/2}^{-4}) \otimes \nu(g_{9/2}^{-2}, g_{7/2}^1)$ configuration. Due to poor statistics, experimental spin assignments were not possible for a series of levels connected to the positive-parity sequence. Comparing their observed energies and decay/feeding patterns with the calculations, these levels at 6945, 10764, 11943, and 12229 keV would correspond to the calculated levels $33/2_2^+$, $43/2_2^+$, $45/2_2^+$, and $47/2_1^+$, respectively.

[1]Only the occupancy of the "active" (not fully occupied or completely empty) orbitals is represented as $\pi(l_j^n, \ldots) \otimes \nu(l'^{n'}_{j'}, \ldots)$.

TABLE II. Relative intensities of γ transitions (I_γ) and half-lives ($T_{1/2}$) calculated for states with decays involving parity-changing transitions, compared to experimental data of ^{95}Pd (present work), ^{95}Rh [26], and ^{94}Ru [26].

Nucleus	E_x^{exp} (keV)	$T_{1/2}^{exp}$	$T_{1/2}^{SM}$	E_γ^{exp} (keV)	σL	$J_i^{\Pi_i} \rightarrow J_f^{\Pi_f}$	I_γ^{exp} (%)	I_γ^{SM} (%)
^{95}Pd	4753		31 ps	681	$E2$	$33/2_1^+ \rightarrow 29/2_1^+$	100(5)	100
				421	$E1$	$\rightarrow 31/2_1^-$	6(2)	2
	4363		111 ps	1666	$E1$	$27/2_1^- \rightarrow 25/2_1^+$	100(25)	48
				458	$E2$	$\rightarrow 23/2_1^-$	17(5)	100
				291	$E1$	$\rightarrow 29/2_1^+$	n.o.	1
				286	$E1$	$\rightarrow 27/2_1^+$	18(8)	4
	4332	11.2(7) ns	7.3 ns	1635	$E3$[a]	$31/2_1^- \rightarrow 25/2_1^+$	4(1)	1
				261	$E1$	$\rightarrow 29/2_1^+$	100(2)	100
	3905		0.52 ps	2029	$E1$	$23/2_1^- \rightarrow 21/2_1^+$	100(29)	71
				1338	$E1$	$\rightarrow 23/2_1^+$	n.o.	5
				1227	$E2$	$\rightarrow 19/2_1^-$	35(15)	100
				1208	$E1$	$\rightarrow 25/2_1^+$	n.o.	0
				297	$M1+E2$	$\rightarrow 21/2_1^-$	33(5)	94
	2202		3.0 ns	323	$E1$	$17/2_1^- \rightarrow 17/2_1^+$	100(9)	100
				229	$E1$	$\rightarrow 15/2_1^+$	28(6)	24
^{95}Rh	8395	1.86(9) ps	1.69 ps	770	$E1$	$35/2_1^- \rightarrow 35/2_1^+$	10(4)	2
				549	$M1+E2$	$\rightarrow 33/2_1^-$	100(7)	100
	2236	18.8(10) ns	13.2 ns	169	$E1$	$17/2_1^- \rightarrow 17/2_1^+$	100	100
^{94}Ru	2624	0.51(5) ns	0.39 ns	438	$E1$	$5_1^- \rightarrow 4_1^+$	100(3)	100
				127	$E1$	$\rightarrow 6_1^+$	46(2)	1
	4489	0.76(4) ns	0.99 ns	498	$E1$	$11_1^- \rightarrow 10_1^+$	100(1)	100
				292	$E2$	$\rightarrow 9_2^-$	47(1)	22
				151	$E2$	$\rightarrow 9_1^-$	1.7(2)	4

[a]Calculated with $e_{\pi,\mathrm{eff}} = +1.5e$ and $e_{\nu,\mathrm{eff}} = +0.5e$.

On the negative-parity side at higher energies, the calculated levels $33/2_1^-$ and $35/2_1^-$ are dominated by the fully stretched configurations $\pi(p_{3/2}^{-1}, g_{9/2}^{-3}) \otimes \nu(g_{9/2}^{-1})$ and $\pi(f_{5/2}^{-1}, g_{9/2}^{-3}) \otimes \nu(g_{9/2}^{-1})$, with contributions of 59% and 87%, respectively. The calculated states $37/2_1^-$, $39/2_{1,2}^-$, and $41/2_{1,2}^-$ are predicted to have more complex structures, strongly mixed, with a few competing configurations such as $\pi(p_{1/2}^{-1}, g_{9/2}^{-3}) \otimes \nu(g_{9/2}^{-2}, d_{5/2}^{1})$, $\pi(p_{1/2}^{-1}, g_{9/2}^{-3}) \otimes \nu(g_{9/2}^{-2}, g_{7/2}^{1})$, $\pi(g_{9/2}^{-4}) \otimes \nu(g_{9/2}^{-2}, h_{11/2}^{1})$, $\pi(p_{1/2}^{-1}, g_{9/2}^{-4}, d_{5/2}^{1}) \otimes \nu(g_{9/2}^{-1})$, and $\pi(p_{1/2}^{-1}, g_{9/2}^{-4}, g_{7/2}^{1}) \otimes \nu(g_{9/2}^{-1})$. The $43/2_1^-$ state is calculated to have a 93% contribution from the completely aligned configuration $\pi(p_{1/2}^{-1}, g_{9/2}^{-3}) \otimes \nu(g_{9/2}^{-2}, d_{5/2}^{1})$, while the calculated levels $43/2_2^-$ and $45/2_1^-$ are almost pure members of the stretched $\pi(p_{1/2}^{-1}, g_{9/2}^{-3}) \otimes \nu(g_{9/2}^{-2}, g_{7/2}^{1})$ structure. The experimental level $45/2^-$ at 10667 keV decays to the only experimentally observed state with spin and parity $43/2^-$ (at 10267 keV), which would better correspond to the second predicted level $43/2_2^-$, as its observed decay and feeding patterns follow better the predictions for the $43/2_2^-$ level.

In ^{95}Pd, several $E1$ transitions were observed to connect different-parity levels below 5 MeV, competing in same cases with the usually faster $M1/E2$ transitions from the some initial levels. Some of these $E1$ transitions also played a vital role in the experimental determination of the excitation energy of the $21/2^+$ spin-gap isomer [10]. In general, low-energy electric dipole transitions in stable spherical nuclei are very hindered, with $B(E1) < 10^{-4}$ W.u. in medium-heavy nuclei, and are understood as originating from small admixtures in the initial and final states. Such small wave-function components could be generated by collective vibrational modes or by single-particle configurations connected by the $E1$-transition operator. In order to explore the latter possibility, the configuration space used in this work included 1p-1h excitations, relative to the dominant configurations of the calculated wave functions. To test our approach, the known spectroscopic characteristics of states deexciting through $E1$ transitions in the neighboring nuclei ^{95}Rh and ^{94}Ru [26] were also compared with theoretical predictions using a similar truncation scheme. The reduced transition probabilities $B(E1)$, $B(M1)$, and $B(E2)$ calculated for the transitions depopulating the states of interest have values of about 10^{-7}–10^{-5}, 0.1–0.5, and 1–8 W.u., respectively. The γ-transition intensities and half-lives calculated for these states with decays involving $E1$ transitions (see Table II) are in good general agreement with the corresponding experimental values and

reproduce reasonably well the competing decay patterns of the transitions with different multipole character ($\sigma L = E1$, $M1$, and $E2$) observed in the deexcitations of the states $23/2^-$ (^{95}Pd), $27/2^-$ (^{95}Pd), $33/2^+$ (^{95}Pd), $35/2^-$ (^{95}Rh), and 11^- (^{94}Ru).

V. CONCLUSIONS

The level scheme of the ^{95}Pd nucleus, investigated with the ^{58}Ni(^{40}Ca,$2pn$) reaction at 135 MeV, was extended up to excitation energies of about 12 MeV. Two bandlike structures were found, one built above the known isomeric $31/2^-$ state at 4332 keV, which extends up to a $45/2^-$ state at 10667 keV, and the other built above the $33/2^+$ state at 4753 keV, reported before [10] and going up to about 12 MeV excitation, with the highest state with assigned spin/parity of $45/2^+$ at 10424 keV. The half-life of the $31/2^-$ isomer was also investigated by means of delayed coincidences, and the measured value of 11.2(7) ns agrees with the previously reported one, 12(3) ns.

Shell-model calculations, considering a truncated model space built upon the $\pi\nu(f, p, g, d, s, h_{11/2})$ orbitals, were performed with the OXBASH code, and they predict excitation energies in fair agreement with the experimental observations. The structure of low-lying yrast and near-yrast levels, with energies below 5 MeV, is strongly dominated by excitations within the $\pi(p_{1/2}, g_{9/2})$ and $\nu g_{9/2}$ orbitals. At higher energies, the calculated high-spin states have dominant configurations with protons and neutrons in the same orbitals, $\pi(p_{1/2}, g_{9/2})$ and $\nu g_{9/2}$, coupled to either one proton hole in the $\pi f_{5/2}$ orbital or one neutron in the $\nu d_{5/2}$ or $\nu g_{7/2}$ orbitals. Configurations with one particle or hole in the other orbitals, $\pi(f_{7/2}, p_{3/2}, g_{7/2}, d, s, h_{11/2})$ and $\nu(f, p, d_{3/2}, s, h_{11/2})$, add relatively modest contributions to the calculated wave functions in most cases. However, 1p-1h excitations within all these orbitals can generate configurations that are coupled by the $E1$-transition operator and can account for much of the strength of $E1$ transitions observed experimentally between levels in ^{95}Pd and in the nearby nuclei ^{95}Rh and ^{94}Ru.

ACKNOWLEDGMENTS

This work was partially supported by UEFISCDI-Romania under program PN-II-IDEI Contract No. 127/2011 and by BMBF (Contract No. 06DA9036I) and HIC for FAIR.

[1] D. H. Gloekner and F. J. D. Serduke, Nucl. Phys. A **220**, 477 (1974).
[2] R. Gross and A. Frenkel, Nucl. Phys. A **267**, 85 (1976).
[3] K. Ogawa, Phys. Rev. C **28**, 958 (1983).
[4] I. P. Johnstone and L. D. Skouras, Phys. Rev. C **55**, 1227 (1997).
[5] I. P. Johnstone and L. D. Skouras, Eur. Phys. J. A **11**, 125 (2001).
[6] E. Nolte and H. Hick, Z. Phys. A **305**, 289 (1982).
[7] S. E. Arnell, D. Foltescu, H. A. Roth, Ö Skeppstedt, J. Blomqvist, A. Nilsson, T. Kuroyanagi, S. Mitarai, and J. Nyberg, Phys. Rev. C **49**, 51 (1994).
[8] M. Gorska *et al.*, Z. Phys. A **353**, 233 (1995).
[9] M. Gorska, R. Schubart, H. Grave, J. B. Fitzgerald, D. B. Fossan, J. Heese, K. H. Maier, M. Rejmund, and K. Spohr, Acta Phys. Pol. B **27**, 165 (1996).
[10] N. Mărginean, D. Bucurescu, C. Rossi-Alvarez *et al.*, Phys. Rev. C **67**, 061301(R) (2003).
[11] D. Bazzacco, Proc. Int. Conf. Nuclear Structure at High Angular Momentum, Ottawa, p.376 (1992), Atomic Energy of Canada Limited (AECL) Report 10613.
[12] C. Rossi-Alvarez *et al.* (unpublished).
[13] E. Farnea *et al.*, Nucl. Instrum. Meth. Phys. Res. A **400**, 87 (1997).
[14] M. Piiparinen *et al.*, Nucl. Phys. A **605**, 191 (1996); N. H. Medina *et al.*, *ibid.* **589**, 106 (1995).
[15] C. Rusu *et al.*, Eur. Phys. J. A **44**, 31 (2010).
[16] I. P. Johnstone *et al.*, J. Phys. G **18**, 1401 (1992).
[17] A. Etchegoyen, W. D. M. Rae, and N. S. Godwin, OXBASH code (MSU version by B. A. Brown, 1986); B. A. Brown, A. Etchegoyen, and W. D. M. Rae, MSUCL Report No. 524, 1986 (unpublished).
[18] J. P. Schiffer and W. W. True, Rev. Mod. Phys. **48**, 191 (1976).
[19] D. H. Gloeckner and R. D. Lawson, Phys. Lett. B **53**, 313 (1974).
[20] T. Otsuka, T. Suzuki, M. Honma *et al.*, Phys. Rev. Lett. **104**, 012501 (2010).
[21] I. G. Darby *et al.*, Phys. Rev. Lett. **105**, 162502 (2010).
[22] G. A. Leander, J. Dudek, W. Nazarewicz, J. R. Nix, and Ph. Quentin, Phys. Rev. C **30**, 416 (1984).
[23] V. I. Isakov, K. I. Erokhina, H. Mach, M. Sanchez-Vega, and B. Fogelberg, Eur. Phys. J. A **14**, 29 (2002).
[24] A. F. Lisetskiy, B. A. Brown, M. Horoi, and H. Grawe, Phys. Rev. C **70**, 044314 (2004).
[25] R. Machleidt, Phys. Rev. C **63**, 024001 (2001).
[26] ENSDF at NNDC (database version of March 14, 2012), http://www.nndc.bnl.gov/ensdf.